Photoproduction of Positive Pions at Backward Angles in the Energy Range 1–3 GeV†

R. A. Alvarez,* G. Cooperstein,‡ K. Kalata,§ R. C. Lanza, and D. Luckey
Department of Physics and Laboratory for Nuclear Science, Massachusetts Institute of Technology, Cambridge, Massachusetts 02139
(Received 10 November 1969)

The cross section for photoproduction of single π^+ from hydrogen has been measured at laboratory angles of 110°, 127.5° and 152°, between 0.9- and 3.2-GeV incident photon energy. Measurements have been made with approximately 15% statistical accuracy at about 40 photon energies at each angle. The results agree well with the previous Caltech data of Thiessen. The cross section shows a rapid drop with increasing energy with superimposed bumps or shoulders corresponding to the $N(1688)$, $\Delta(1920)$, and $\Delta(2420)$. A shallow minimum is observed at the $N(2190)$ resonance.

I. INTRODUCTION

A CONSIDERABLE amount of theoretical and experimental work has been done in the past few years on single-pion photoproduction with incident photon energy greater than 1 GeV.[1] In general, most of this work has been done at small center-of-mass angles; the DESY,[2] Cornell,[3] CEA,[4] and SLAC[5] data on π^0 photoproduction, and the Caltech[6] data on π^+ photoproduction, were the only large center-of-mass-angle results available until this experiment. SLAC[7] data and the data reported in this paper greatly extend our knowledge of π^+ photoproduction and should be of some theoretical interest.

In this experiment a single-arm magnetic spectrometer with wide-gap spark chambers was used to measure the single-π^+ photoproduction cross sections from hydrogen at laboratory production angles of 110°, 127.5°, and 152°, between 0.9- and 3.2-GeV photon energy. In this energy region, resonances in the direct channel appear to make a large, and perhaps dominant, contribution to the amplitude. The results agree well at the lower energies with the previous Caltech data, and at the higher energies with the recent SLAC data.

This paper is divided into four parts. Section II describes the nature of the experiment and the apparatus and techniques used to obtain the data. The techniques of scanning and analyzing the data are described in Sec. III. Finally, the experimental results and their analysis are presented in Sec. IV.

II. EXPERIMENTAL METHOD

A. General Considerations

A collimated bremsstrahlung beam from the Cambridge electron accelerator was incident on a liquid-hydrogen target. The production angle and momentum of positive pions produced in the target were measured by means of a magnetic spectrometer. A single measurement of pion angle and momentum is sufficient to determine the incident photon energy for single-pion production. In the case of multiple-pion production, a lower limit on the photon energy can be obtained by assuming that the undetected pion is produced at rest. The photon energy computed with this restriction is always several hundred MeV above the photon energy computed under the assumption of single-pion production. Hence there is a range of several hundred MeV in photon energy extending down from the end of the bremsstrahlung spectrum in which single-pion photoproduction can be kinematically separated from multiple-pion production. This is illustrated in Fig. 1 for one particular pion angle. Because of the limited useful energy region below the maximum energy E_0, data for photon energies from 0.9 to 3.0 GeV were taken at six different values of E_0. Each useful energy region overlapped the ones above and below it, and data in each region were taken on several separate runs spaced over a period of several days and separated by runs at other energies.

The spectrometer angular acceptance at any particular angular setting was approximately 15° in the laboratory. Data were taken at nominal spectrometer angles of 110°, 127.5°, and 152°.

† Work supported in part by U. S. Atomic Energy Commission, under Contract No. AT(30-1)-2098. This work is based on a dissertation submitted by G. Cooperstein in partial fulfillment of the requirements for a Ph.D. in Physics from MIT (1968).
* Present address: Lawrence Radiation Laboratory, Livermore, Calif.
‡ Present address: Ion Physics Corporation, Burlington, Mass.
§ Present address: Center for Space Research, MIT, Cambridge, Mass.

[1] A review including references is given by B. Richter, in *Proceedings of the Third International Symposium on Electron and Photon Interactions at High Energies, Stanford Linear Accelerator Center, 1967* (Clearing House of Federal Scientific and Technical Information, Washington, D. C., 1968), p. 309.
[2] G. Buschorn, P. Heide, U. Kötz, R. A. Lewis, P. Schmüser, and H. J. Skronn, Phys. Rev. Letters **20**, 230 (1968).
[3] G. L. Cassiday, H. Fisher, A. Ito, E. C. Loh, and J. Rutherfoord, Phys. Rev. Letters **21**, 933 (1968); also E. C. Loh (private communication).
[4] J. R. Uglum, Jr., Ph.D. thesis, MIT, 1965 (unpublished). See also G. C. Bolon, D. Garelick, S. Homma, R. Lewis, W. Lobar, D. Luckey, L. S. Osborne, R. Schwitters, and J. Uglum, Phys. Rev. Letters **18**, 926 (1967).
[5] D. Tompkins, R. Anderson, B. Gittelman, J. Litt, B. H. Wiik, D. Yount, and A. Minten, Phys. Rev. Letters **23**, 725 (1969).
[6] H. A. Thiessen, Phys. Rev. **155**, 1488 (1967).
[7] R. L. Anderson, D. Gustavson, J. Johnson, I. Overman, D. Ritson, and B. H. Wiik, Phys. Rev. Letters **23**, 721 (1969).

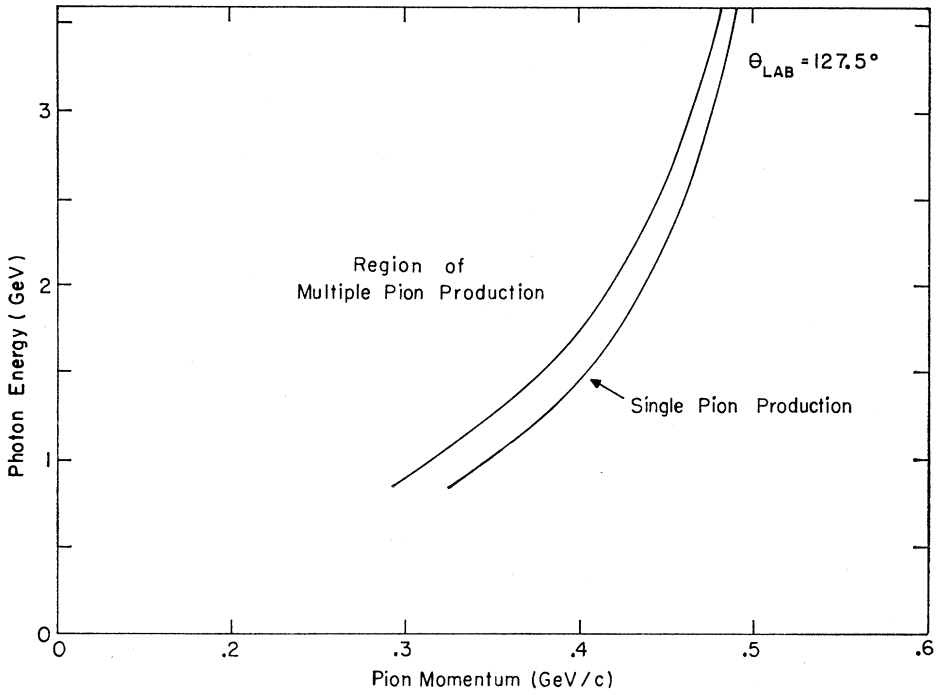

FIG. 1. Photon energy needed to produce a single pion and minimum photon energy needed to produce two pions, as a function of pion momentum at $\theta_{lab}=127.5°$.

B. Bremsstrahlung Beam and Hydrogen Target

A plan view of the experiment is shown in Fig. 2. The CEA electron beam irradiated either a 0.0026-radiation-length beryllium radiator or a 0.0710-radiation-length tungsten radiator. The tungsten radiator was used only when the cross section was so low as to preclude a reasonable counting rate with the beryllium radiator. The resulting photon beam was collimated by a 0.125-in. square Hevimet collimator subtending an angle of 0.230 mrad. Sweeping magnets after the collimator removed charged secondaries, and two scrapers placed before the hydrogen radiator reduced the beam halo. The beam flux was measured by a thin-walled ionization chamber and a multigap quantameter.[8] The average currents from the ionization chamber and the quantameter were recorded for each run during the experiment. At a given electron beam energy E_0, the ratio of these currents remained constant to better than 1%.

The shape of the photon spectrum for each E_0 was calculated by a computer program written by Wolverton.[9] This program combined the effects of showering and multiple scattering in the radiator to obtain a bremsstrahlung spectrum averaged over the angular distribution of the collimated beam. It is expected that the results of this program are accurate to better than 2%. In order to reduce possible systematic errors due to uncertainties in the shape of the spectrum near the upper end, however, we restrict our useful energy range to energies below $0.97E_0$. The bremsstrahlung spectra calculated by this program for the two different radiators and for $E_0=1.2$ and 3.0 GeV are shown in Fig. 3.

The liquid-hydrogen target consisted of a Mylar cell 7.5 in. long and 2 in. in diameter supported inside a vacuum chamber with 0.005-in. Mylar windows for the beam and 0.007-in. windows for the photoproduced pions. The beam spot was 0.5×0.5 in. at the hydrogen target and was centered to within 0.125 in. of an axial line extending through the target with the use of Polaroid beam pictures.

C. Spectrometer Magnet

A circular magnet with 32-in. diam pole faces and a 3-in. gap was used for momentum analysis. The magnet acted as a crude lens, focusing pions of a given momentum and different production angles into a small region of the rear spark chambers. The magnet current was regulated to ±0.05% and was recorded before and after each run along with the readings from a rotating coil gaussmeter permanently mounted 4 in. from the center of the magnet. In order to be able to reproduce a magnetic field by setting the magnet current, great care was taken in changing magnetic field so as to remain always on the same hysteresis curve. During the experiment the gaussmeter was periodically calibrated against a standard permanent magnet, and at the end of the experiment the spectrometer magnet was set to the current values used during the data runs while the gaussmeter was calibrated against a nuclear-magnetic-resonance probe.

[8] G. F. Dell and M. Fotino, CEA Report No. CEAL-1040, 1968 (unpublished).
[9] F. Wolverton (private communication).

Because the field shape varied slightly with the value of the central magnetic field, the field profile was mapped at 16, 18, and 20 kG. During the experiment the central field varied between about 13 kG for our lowest beam energy to 20 kG for our highest; the field profile used in the momentum analysis was an extrapolation or interpolation of the three measured profiles.

D. Scintillation Counters

Four scintillation counters were used to detect the pions. Lead bricks shielded counter S_1 from particles not coming from the hydrogen target, and in addition at the two forward spectrometer angles S_1 was covered with 0.25 in. of carbon to reduce the high flux of low-energy particles. The phototubes on all counters were shielded from the fringe field of the magnet. Some reduction in phototube gain was noted, particularly at high magnetic field. The phototube voltages and discriminator biases were therefore set at the highest magnetic field, so that at lower magnetic fields these settings were conservative. The position of counter S_4 was chosen at each spectrometer angle to exclude most low-momentum pions which otherwise would have triggered our system. Finally, 0.75 in. of copper absorber placed in front of counters S_2 and S_3 and 0.2 in. of stainless steel placed between them eliminated all protons of momentum less than 565 MeV/c and reduced the coincidence rate between these two counters.

E. Logic Circuitry

A photoproduced pion generated a fourfold coincidence of the discriminator outputs. This coincidence

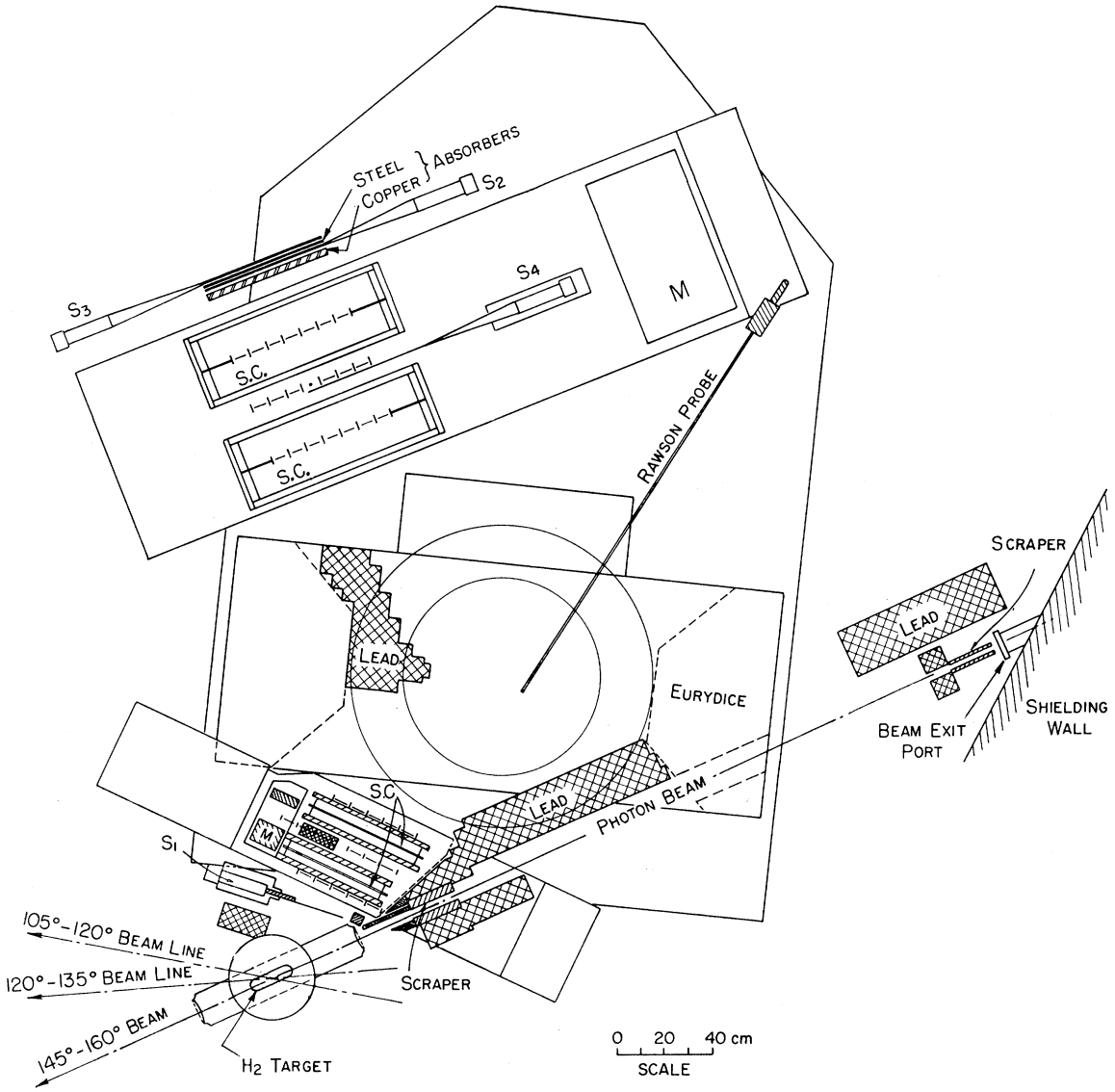

FIG. 2. Plan view of experimental apparatus.

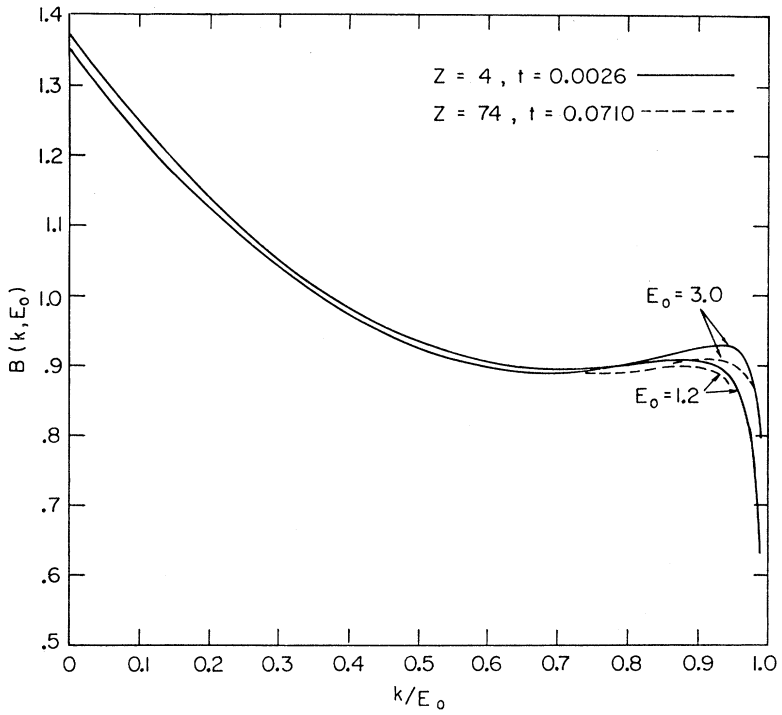

FIG. 3. Bremsstrahlung intensity $B(k,E_0)$ for the two radiators used in this experiment, shown for $E_0=1.2$ and 3.0 GeV.

activated the gating circuitry, triggered the spark chambers, and flushed the fiducial rulers, binary lights, and digital lights inside the optical systems and then advanced the film. During the advance the triggering logic was gated off. A block diagram of the logic circuitry is shown in Fig. 4.

Our fast-logic system was composed of conventional tunnel diode coincidence circuits and discriminators, with limiter circuits placed in front of the discriminators in order to prevent damage to them by pickup from the spark-chamber discharges. In order to be able to correct for chance coincidences in which one particle triggered one or more counters and another triggered the rest within the 25-nsec resolving time of the coincidence network, several combinations of coincidences and delayed coincidences ("accidentals") between the four scintillation counters were monitored. The delayed coincidences were also allowed to trigger the system so that we could determine what this type of event looked like on film.

Both slow- and fast-gated scalers were used in monitoring coincidences. The slow-gated scalers as well as the spark-chamber trigger were gated off during the camera advance (about 330 msec). The fast scalers were gated off for 8 msec—sufficient time to avoid pickup due to spark chamber rf, but less than the 16 msec between two beam pulses. Since the beam pulse duration was always less than 8 msec, the gating allowed no more than one count per beam pulse.

F. Spark Chambers

The pion's trajectory was recorded by photographing the tracks it produced in two sets of wide-gap spark chambers placed before and after the magnet. Each of the front chambers had two 1.5-in.-wide gaps, and those in the rear had two 5-in. gaps each. Two Marx generators were used to apply to the spark chambers a voltage pulse of approximately 10 kV/cm with a 10-nsec rise time and 200-nsec duration. The Marx generators consisted of six capacitor banks charged in parallel through resistors with a large RC time constant and discharged in series through triggered spark gaps so that the output voltage was approximately six times the input voltage. The short rise time minimizes coherent drift of the electrons away from the negatively charged plate and increases spark-chamber efficiency in high backgrounds.

G. Optical Systems

The spark chambers before and after the magnet were viewed by separate optical systems. In each system, field lenses, large prisms, mirrors, and a 35-mm camera were arranged so as to provide two orthogonal views of the spark chambers on a single frame of film. Television cameras placed below the 35-mm cameras allowed the events to be observed as they occurred.

Fiducial rulers, flashed simultaneously with the spark chambers, provided an array of cross marks from which spark positions could accurately be measured. Binary and digital lights were used to record on film relevant

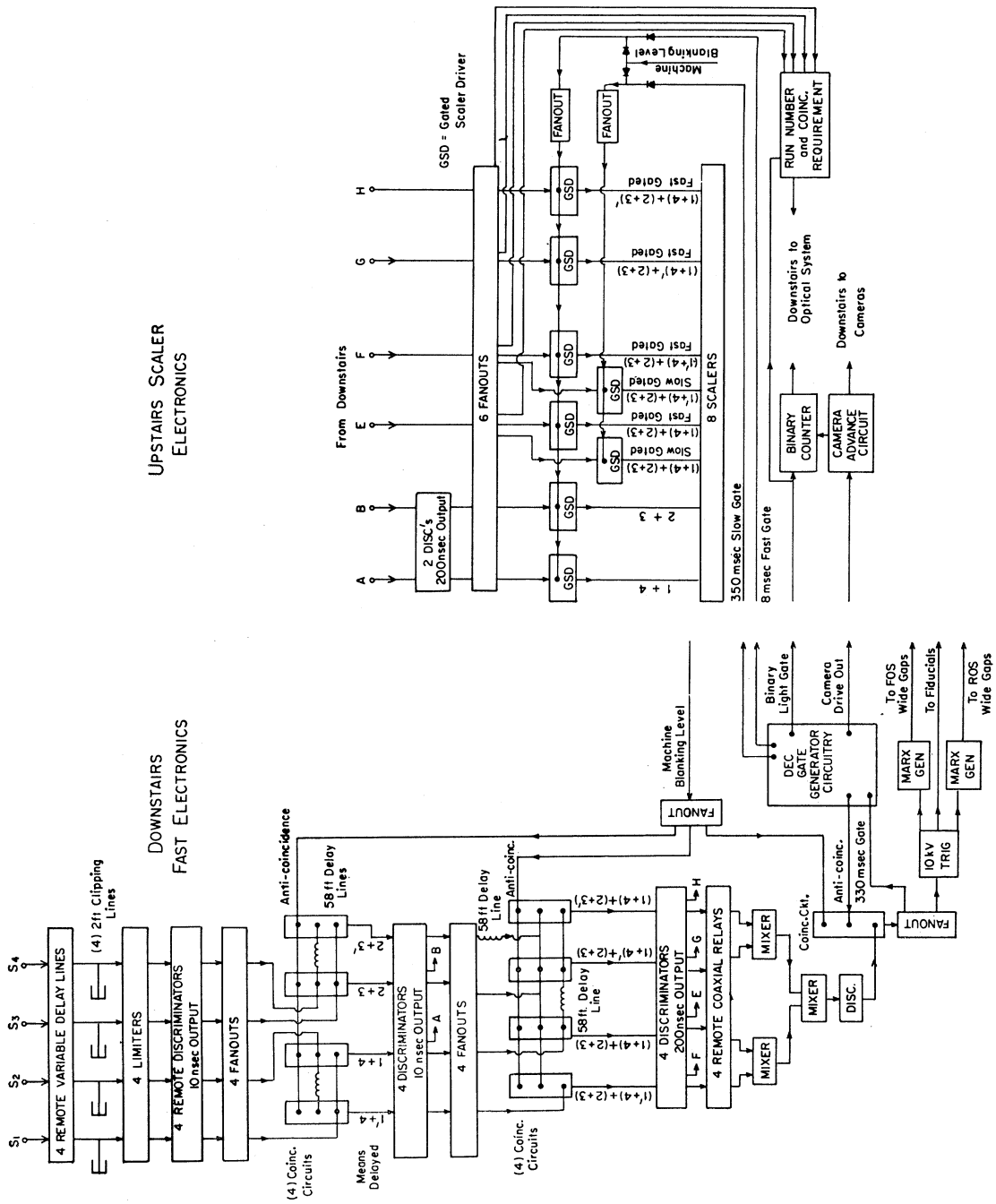

FIG. 4. Block diagram of the electronics showing the combinations of real and accidental events monitored in this experiment.

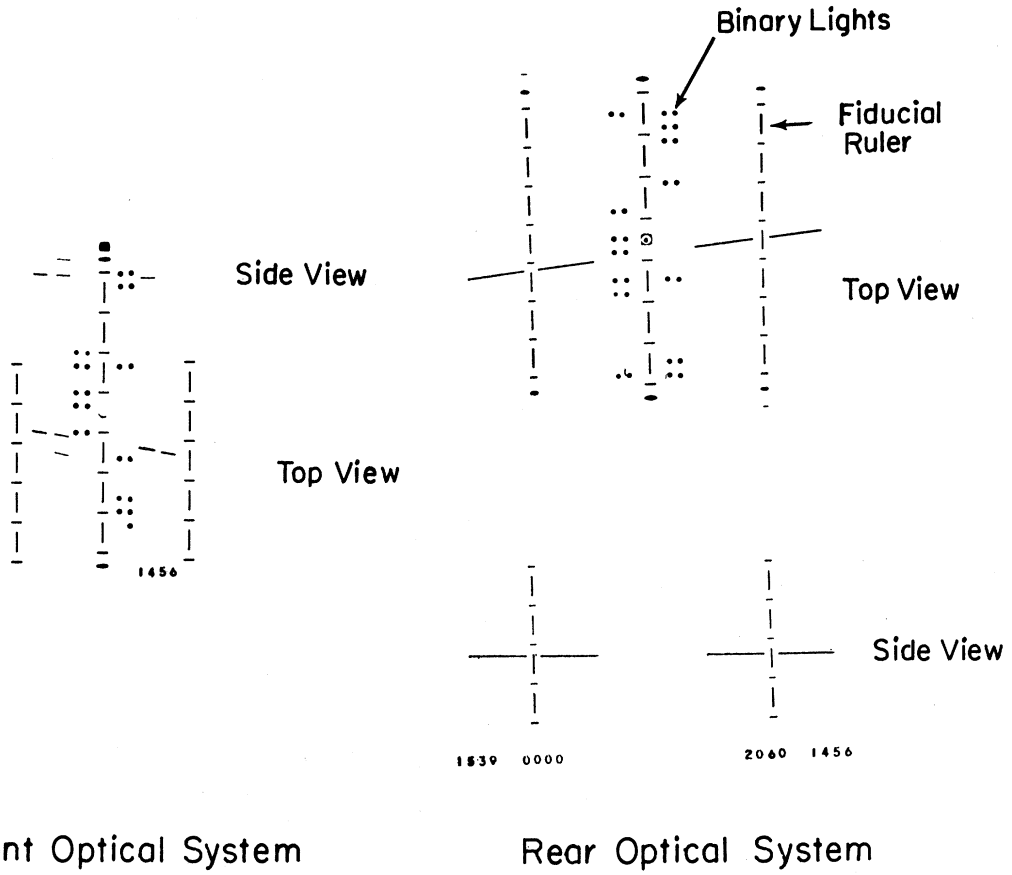

FIG. 5. Typical event as photographed in the front and rear optical systems showing operation of wide-gap chambers.

information about each event. Figure 5 shows a picture of a typical event in both optical systems.

The optical systems were carefully aligned so that we photographed a plane parallel to the horizontal to within $\pm 0.03°$. With the spark chambers removed, but fiducials in place, photographs were taken of strings run through the optical systems at various angles from the center of the magnet and from several points displaced known distances from the center. The real-space angles of these strings were measured with a theodolite. These pictures were used to determine the transformation from film space to real space, and were helpful in understanding the aberrations associated with spherical optics and our methods of viewing the spark chambers.

H. Backgrounds

In preliminary runs a high-momentum proton background many times larger than the pion flux was discovered. 0.75 in. of copper absorber placed in front of counters S_2 and S_3 eliminated these protons, and also stopped approximately 10% of the pions. The nuclear absorption was calculated as a function of pion momentum using measured π^+ and π^- cross sections and used as a correction in the data analysis.

Empty-target data were taken periodically, and subsequent analysis showed that the empty-target background had a negligible effect on our cross sections. More than 95% of the empty-target events came from the end caps of the hydrogen target and in the final data analysis were eliminated by appropriate cuts on the event origin in the target. Figure 6 shows a distribution of empty-target events in the target cell. Positron contamination was shown to be negligible by reversing the magnetic field and looking at the associated electrons. The only contamination not observed directly was muon contamination, mainly resulting from pion decays occurring between the target and the spectrometer. Calculations showed this background to be negligible.

III. DATA ANALYSIS

A. Picture Scanning

The spark-chamber photographs taken during the experiment were scanned and measured by the computer scanning system SPASS on a PDP-1 computer.[10,11] This

[10] M. Deutsch, IEEE Trans. Nucl. Sci. **NS12**, 69 (1965).

[11] M. Deutsch, in *Proceedings of the Conference on Photon Interactions in the BeV Energy Range*, edited by B. T. Feld (MIT Laboratory of Nuclear Science, Cambridge, Mass., 1963), p. VII.18.

scanning system was used to locate the spark segments on film and to record their positions and angles, relative to the fiducial rulers, on magnetic tape. The film from each optical system was scanned separately and the tapes later merged and analyzed on an IBM 360/65 computer. After the SPASS system was properly calibrated for the geometry of this experiment, scanning time, including film loading time, was less than 3 sec for each frame of film, or 6 sec for each event. Approximately 1% of the film was scanned visually by physicists as a check on the computer scanning results.

The SPASS scanning efficiency was generally less than 100% because of faint tracks in the chambers near the target. Especially at the higher beam energies, there were often several background tracks which robbed from the primary tracks. The efficiency for locating good tracks in the front optical system varied between 82 and 99%, depending on the energy of the beam and the spectrometer angle.

Since the efficiency for detecting good tracks in the rear chamber was 100%, the events in which a track in the front system was not detected by SPASS could be determined. The robbing in the front chambers was basically random in nature, so that only events in which good tracks were measured in both optical systems were analyzed, and the results of this analysis were weighted by the ratio of the total number of good events found in the rear chamber to the number of events analyzed.

The final scanning accuracy obtained was ± 0.04 in. in real-space position, $\pm 0.35°$ in angle in the front optical system, and $\pm 0.25°$ in angle in the rear optical system.

B. Event Reconstruction

1. Spatial Reconstruction

In order to calculate the incident photon energy, it was necessary to measure the pion production angle and momentum. The production angle was determined directly from the front optical system pictures, while the momentum was calculated from the amount of bending in the magnetic field. Since the momentum could be calculated from an angle and position in one optical system, and a position in the other, the momentum was overdetermined. In our calculations we used the total bending angle and the impact parameter (the perpendicular distance from the center of the magnet to the extrapolation of the trajectory of the pion before it enters or leaves the magnetic field) as measured in each optical system as variables. The requirement that the impact parameter measured in each system be equal allowed us to eliminate almost all bad events.

The calibration constants necessary for determining the bending angle, production angle, and impact parameter of the particles were easily determined from film measurements of string photographs referred to in Sec. II G. Uncertainties in these constants caused systematic errors of less than $\pm 0.15°$ in production angle, $\pm 0.2°$ in bending angle, and ± 0.1 in. in impact parameter.

The final accuracies obtained for actual events were limited by SPASS measurement precision rather than by the calibration constants and were $\pm 0.4°$ in bending angle and $\pm 0.35°$ in production angle.

2. Pattern Recognition

For good events, SPASS found all four spark segments in the rear optical system 95% of the time and at least two segments the remaining 5% of the time. A second spark track was found in one or more gaps in less than 5% of the frames and was always easily rejected as not corresponding to a good particle trajectory. "Accidental" frames were either blank or had a track that was easily rejected as not coming from the target.

The front optical system was more difficult to analyze the rear system because it often had several tracks with one or more missing gaps per track. A program was written to link together the spark segements into tracks and to determine which track was produced by the particle of interest. This program linked together all collinear combinations of two or more spark segments in different gaps and matched the track in the rear

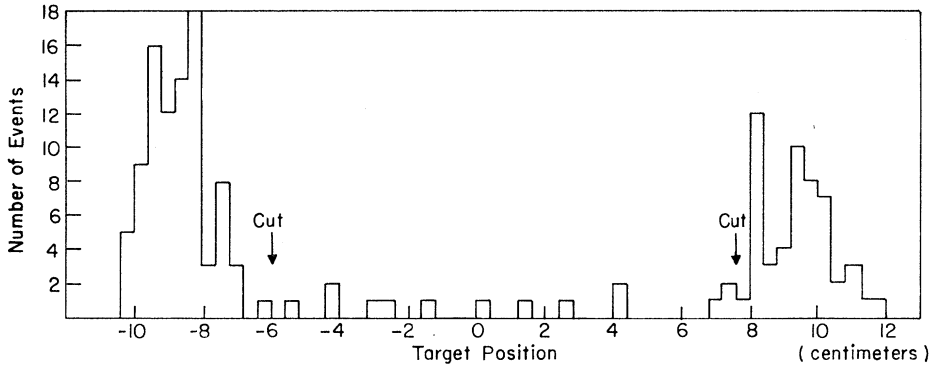

FIG. 6. Histogram of empty-target data showing the position of the cuts used to eliminate events produced in the end caps of the hydrogen cell.

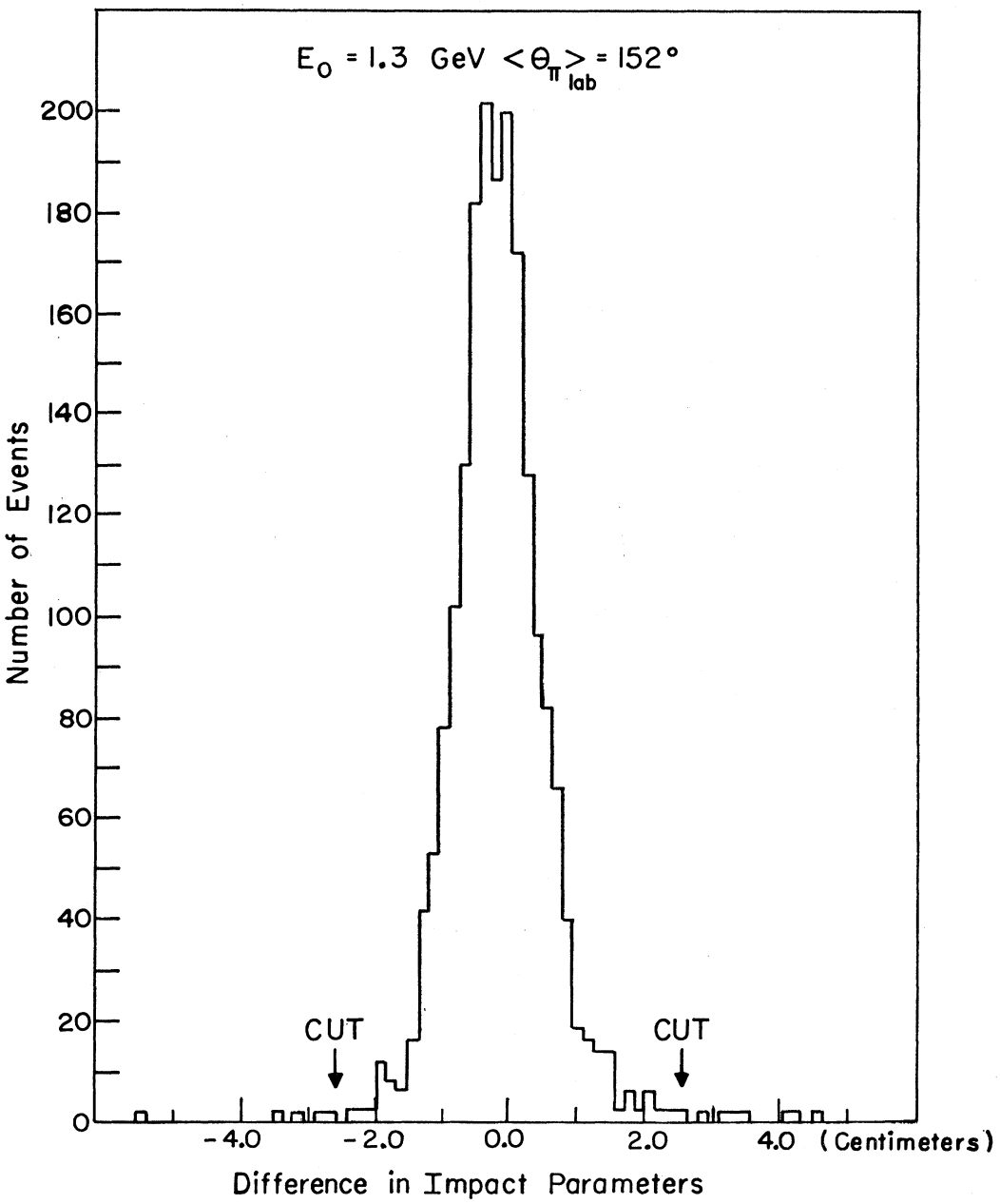

FIG. 7. Histogram of the difference in the impact parameters measured in the front and rear optical systems showing the cuts imposed on this difference to eliminate particles which scattered off the magnet pole faces or decayed in flight.

chamber with the track in the front chamber having the same impact parameter.

3. Momentum Determination

The particle momentum was determined by looking up its radius of curvature in a table stored in the computer memory, given its measured impact parameters and bending angle as inputs. The table was generated by an iterative procedure which treated the magnetic field as many concentric rings of constant field strength.[12] The field strength of each ring was determined from the measured radial field profiles. The final momentum resolution of our spectrometer, $\Delta P/P \simeq \pm 0.35\%$, was determined primarily by SPASS measurement precision and uncertainties in the magnetic field.

C. Magnet Acceptance

At each spectrometer setting, events produced from the entire length of the hydrogen target were observed

[12] E. Ritz, B. S. thesis, MIT, 1966 (unpublished).

over a large range of production angles. For production angles above and below this range, only events from part of the hydrogen target could be observed. The length of hydrogen target which was effective in producing observed events was a function of the pion production angle and the incident photon energy. This effective target length was determined by a computer program which traced particles of a given production angle, momentum, and initial position in the hydrogen target through our system and determined whether they lay in the fiducial volume of the spark chamber. All events were weighted by the ratio of maximum length of the hydrogen target to the effective length for the particular type of event.

The magnet acceptance in the vertical plane, $\Delta\Phi$, was calculated assuming that the 3-in. separation of the magnet pole faces was the limiting aperture in the vertical plane. The fringe field of the magnet defocuses the pions at negative impact parameters (small production angles), thus decreasing $\Delta\Phi$, and focuses them at positive impact parameters (large production angles), thus increasing $\Delta\Phi$. This correction which caused $\Delta\Phi$ to vary by as much as 40% over the measured range of impact parameters was included in the calculation of $\Delta\Phi$ for each event. Fortunately, to within measurement accuracy the correction was linear in impact parameter, going to zero as impact parameter went to zero. Since for a typical set of data the impact parameter distribution was both flat and symmetric about zero, the effect of this correction on the final cross sections integrated out to zero when the cross sections were averaged over the range of laboratory production angles analyzed for each run. The average vertical acceptance angle $\Delta\Phi$ was 5.2°, 3.1°, and 2.7°, respectively, at $\langle\theta_\pi\rangle_{\text{lab}} = 152°$, 127°, and 110°.

D. Event Selection

1. Fiducial Volume

Geometrical cuts were applied to all events to insure that they were contained within the acceptable fiducial volume of the spectrometer. Starting with the restriction that the event originated from an acceptable region of the hydrogen target in both the horizontal and vertical planes, the cuts imposed were on the following variables: position along counter S_1, position in the front optical system, position in the magnet (to be certain the particle missed lead shielding bricks), position along counter S_4 in the rear optical system, and position along counters S_2 and S_3.

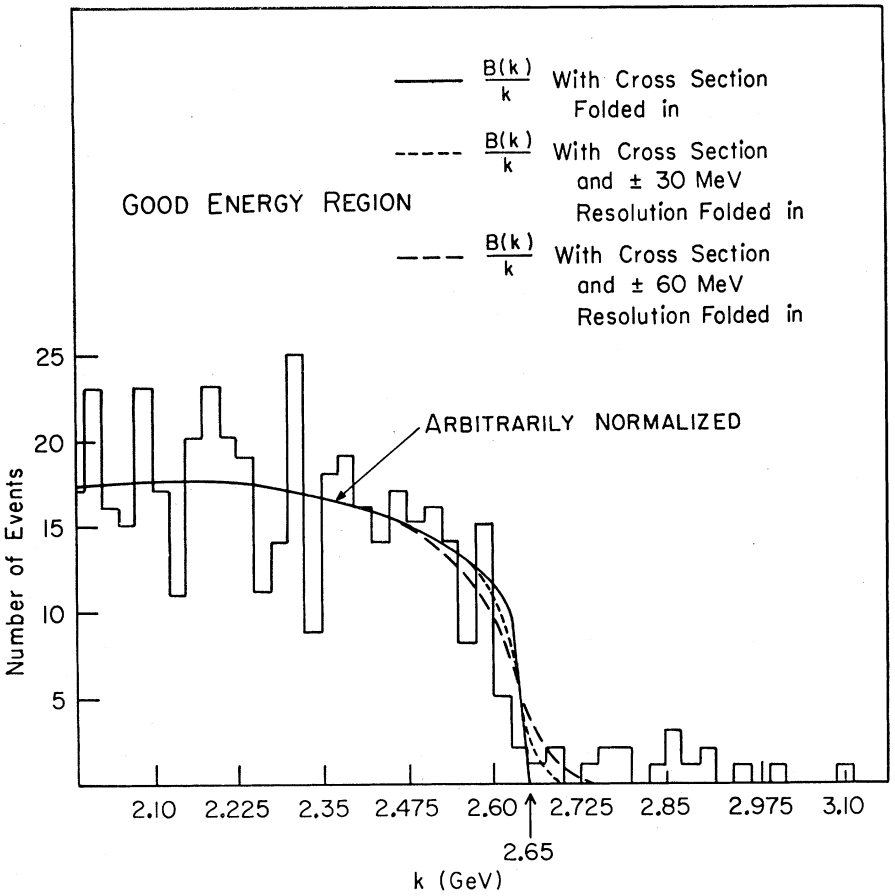

FIG. 8. Uncorrected photon energy distribution (arbitrarily normalized) with the theoretical bremsstrahlung (solid line) spectrum superimposed. The dotted line is the bremsstrahlung spectrum calculated for ±30-MeV/c resolution, and the dashed line is for ±60-MeV/c resolution.

2. *Pion Decays and Scatters*

In order to reject events in which the pion scattered off one of the magnet pole faces or decayed in flight, with the resulting muon continuing through the rest of the system, two consistency requirements were imposed. Because the impact parameters of a particle entering and leaving the magnetic field must be equal, decays or scatters in the horizontal plane were eliminated by imposing cuts on the difference between the impact parameters measured in the front and rear optical systems. A distribution of this difference, showing the location of the cuts, is given in Fig. 7. The width of the distribution is consistent with the SPASS measurement accuracy.

In all cases, the cuts applied to this distribution were greater than 3 standard deviations from the center, thus insuring that a negligible percentage of good events was rejected by this criterion. If the remaining tails of the distribution are extrapolated under the peak, the contamination is less than 2%.

To eliminate scatters or decays which occurred mainly in the vertical plane, the track in the rear optical system was extrapolated back in the vertical plane to the beam line. Those events which extrapolated back to above or below the hydrogen target were eliminated. This extrapolation could not be done exactly because of the fringe field focusing at the edges of the magnet. An approximate correction for this effect could be made, however, which introduced an angular uncertainty less than the $\pm 0.25°$, owing to scanning accuracy. The side view in the front optical system was not used for this correction because, in a number of cases, the correct side view track was difficult to pick out from the background tracks. The vertical target height distribution as measured from the rear optical system is consistent with the 0.5-in. beam width and the $\pm 0.25°$ angular measuring accuracy, especially if one allows for a slight additional broadening caused by uncertainties in the vertical focusing correction. A calculation which traced the muons produced by pion decays through the system showed that these two requirements eliminated more than 90% of all pions which decayed between the spark chambers and still triggered the system.

3. *Kinematics*

The rejection criterion which had the largest effect in limiting the number of events used for the calculation of the final cross sections was the energy cutoff at the inelastic kinematic threshold. This was the requirement that the γ-ray energy required to produce an additional pion along with the observed pion would be beyond the tip of the bremsstrahlung spectrum. To insure this, a lower limit to the pion momentum was placed on all the data from a particular E_0 and spectrometer angle, with a corresponding photon energy cutoff. Most of the data taken at each E_0 came from γ-ray energies below this cut, since the spectrometer acceptance was designed to be 100% efficient over most of the useful γ-ray energies and did not fall sharply to zero outside this region. This, coupled with the rise with decreasing γ-ray energy of both the cross section and the bremsstrahlung spectrum, caused a large number of triggers to come from low-momentum pions.

Our full width at half-maximum (FWHM) energy resolution, estimated from the SPASS scanning accuracy, varies between 10 and 60 MeV, depending on the incident photon energy and spectrometer angle. Calibration errors ($\pm 0.25\%$) in the measurement of the magnetic field introduce a possible systematic photon energy shift of approximately ± 6 MeV at 1 GeV and ± 45 MeV at 3 GeV. These estimates are consistent with the observed energy dependence of the data near the bremsstrahlung cutoff as shown in Fig. 8.

E. Calculation of Cross Section

All the data taken at a given spectrometer angle and primary beam energy (E_0) were binned with respect to γ-ray energy and pion laboratory production angle and were used to calculate a center-of-mass differential cross section for the central energy and angle of each bin. The formula used to derive the cross section for each bin has the following form:

$$\left(\frac{d\sigma}{d\Omega}\right)_{\text{c.m.}} = \frac{kE_0}{B(k)K_q\rho\Delta k\Delta\cos\theta}\eta_1\sum_{i=1}^{N}\frac{\eta_{2i}\eta_{3i}\eta_{4i}\eta_{5i}}{\Delta\Phi_i\Delta z_i(d\Omega^*/d\Omega_i)q_i}.$$

In the above formula,

k = center of γ-ray energy bin,
$B(k)$ = correction for shape of bremsstrahlung spectrum,
K_q = quantameter constant,
$\rho = H_2$ density,
Δk = width of γ-ray energy bin,
$\Delta\cos\theta$ = the difference in $\cos\theta$ over the width of the laboratory production angle bin,
η_1 = correction for events beyond the tip of the bremsstrahlung spectrum ($\sim$0.8–0.99).

The following quantities were separately evaluated for each event. The index i refers to the event number and N is total number of events in a given bin.

η_2 = correction for pions lost due to decay in flight ($\sim$1.18),
η_3 = correction for pions lost due to nuclear absorption ($\sim$1.08–1.14),
η_4 = correction for SPASS scanning efficiency ($\sim$1.03–1.25),
$\Delta\Phi$ = vertical acceptance angle,
Δz = effective H_2 target length,
$d\Omega^*/d\Omega$ = angular Jacobian for conversion from laboratory system to center-of-mass system,
η_5 = correction for pions lost due to dead-time effects ($\sim$1.1–1.25),

TABLE I. Tabulation of center-of-mass cross sections. E_0 is the primary electron beam energy; where more than one value is indicated, data from runs at the different E_0 have been combined. $\langle\theta_\pi\rangle_{\text{lab}}$, $\langle\theta_\pi\rangle_{\text{c.m.}}$, k, and u are the central values of the respective bins, where θ_π is the pion production angle, k is the laboratory system momentum of the incident photon, and u is the square of the four-momentum transfer from photon to nucleon. The laboratory-system bin widths for pion production angle and photon momentum are denoted by $\Delta\theta_{\text{lab}}$ and Δk, respectively.

$\langle\theta_\pi\rangle_{\text{lab}}$ (deg)	k_{lab} (GeV/c)	$\Delta\theta_{\text{lab}}$ (deg)	Δk_{lab} (GeV/c)	E_0 (GeV)	$\langle\theta_\pi\rangle_{\text{c.m.}}$ (deg)	$\langle d\sigma/d\Omega\rangle_{\text{c.m.}}$ (10^{-32} cm^2/sr)	$d\sigma/du$ (10^{-31} [cm/(GeV/c)]^2)	u [(GeV/c)^2]
110.5	0.91	15	0.02	1.2	136.7	366 ±34	417 ±37	0.148
110.5	0.93	15	0.02	1.2	137.0	310 ±32	348 ±36	0.142
110.5	0.95	15	0.02	1.2	137.2	360 ±33	390 ±36	0.135
108.0	0.97	10	0.02	1.2	137.1	353 ±42	370 ±44	0.113
108.0	0.99	10	0.02	1.2	137.4	340 ±40	348 ±41	0.107
108.0	1.01	10	0.02	1.2	137.6	355 ±42	355 ±41	0.100
108.0	1.03	10	0.02	1.2	137.9	267 ±37	259 ±36	0.095
108.0	1.05	10	0.02	1.2	138.1	321 ±43	302 ±41	0.088
108.0	1.07	10	0.02	1.2	138.3	247 ±41	226 ±41	0.082
108.0	1.09	10	0.02	1.2	138.6	179 ±38	161 ±34	0.075
105.5	1.12	5	0.04	1.2	135.6	99 ±30	86 ±26	0.061
109.5	1.24	13	0.04	1.6	140.6	102 ±10	76.8 ± 7.5	0.045
109.5	1.28	13	0.04	1.6	141.0	94 ±10	67.0 ± 7.2	0.035
109.5	1.32	13	0.04	1.6	141.4	1.04±11	73.0 ± 7.6	0.026
109.5	1.36	13	0.04	1.6	141.8	86 ±10	57.4 ± 6.6	0.017
109.5	1.40	13	0.04	1.6	142.2	96 ±11	61.6 ± 6.8	0.009
109.5	1.44	13	0.04	1.6	142.5	95 ±11	58.6 ± 6.7	+0.001
110.5	1.48	13	0.04	1.6, 1.9	142.9	64.4 ± 5.4	38.5 ± 3.2	0.000
110.5	1.52	13	0.04	1.6, 1.9	143.2	67.5 ± 5.8	39.2 ± 3.3	−0.007
111.0	1.56	12	0.04	1.9	144.2	68.6 ± 7.2	38.4 ± 4.0	−0.010
111.0	1.60	12	0.04	1.9	144.5	74.8 ± 7.7	41.0 ± 4.2	−0.018
111.0	1.64	12	0.04	1.9	144.8	46.4 ± 6.2	24.4 ± 3.3	−0.024
111.5	1.68	13	0.04	1.9, 2.1	145.1	46.9 ± 5.0	23.9 ± 2.6	−0.031
111.5	1.72	13	0.04	1.9, 2.1	145.4	38.7 ± 4.6	19.2 ± 2.3	−0.037
111.5	1.76	13	0.04	1.9, 2.1	145.7	24.2 ± 3.7	11.6 ± 1.8	−0.042
111.5	1.80	13	0.04	1.9, 2.1	146.0	26.0 ± 3.9	12.3 ± 1.8	−0.045
111.5	1.84	13	0.04	2.1	146.3	11.7 ± 4.3	5.34± 1.90	−0.050
111.5	1.90	13	0.08	2.1, 2.3	146.7	18.4 ± 2.2	8.15± 0.99	−0.058
111.5	1.98	13	0.08	2.1, 2.3	147.2	8.4 ± 1.5	3.54± 0.65	−0.068
111.5	2.06	13	0.08	2.3	147.7	10.6 ± 2.2	4.29± 0.88	−0.078
112.5	2.14	15	0.08	2.3, 2.65	149.1	7.9 ± 1.1	3.05± 0.43	−0.078
113.0	2.22	12	0.08	2.65	149.8	9.6 ± 1.6	3.56± 0.57	−0.082
113.0	2.30	12	0.08	2.65	150.1	8.8 ± 1.5	3.10± 0.54	−0.091
113.0	2.38	12	0.08	2.65	150.4	6.9 ± 1.4	2.32± 0.49	−0.097
113.5	2.46	12	0.08	2.65, 3.0	151.0	7.1 ± 1.0	2.32± 0.33	−0.060
113.5	2.54	12	0.08	3.0	151.4	8.3 ± 1.2	2.60± 0.37	−0.107
113.5	2.62	11	0.08	3.0	151.8	7.8 ± 1.6	2.35± 0.47	−0.114
113.5	2.70	11	0.08	3.0	152.2	4.4 ± 1.2	1.29± 0.36	−0.119
113.5	2.78	11	0.08	3.0	152.5	6.1 ± 1.6	1.71± 0.43	−0.125
113.5	2.86	11	0.08	3.0	152.9	4.9 ± 1.5	1.34± 0.38	−0.131
127.5	0.89	15	0.02	1.2	148.6	204 ±19	241 ±23	0.220
127.5	0.91	15	0.02	1.2	148.8	225 ±21	257 ±24	0.214
127.5	0.93	15	0.02	1.2	149.0	247 ±19	274 ±22	0.208
127.5	0.95	15	0.02	1.2	149.2	273 ±20	295 ±21	0.203
127.5	0.97	15	0.02	1.2	149.4	268 ±20	281 ±21	0.197
127.5	0.99	15	0.02	1.2	149.6	276 ±20	282 ±21	0.192
127.5	1.01	15	0.02	1.2	149.8	282 ±21	280 ±21	0.188
127.5	1.03	15	0.02	1.2	150.0	220 ±18	213 ±18	0.183
127.5	1.05	15	0.02	1.2	150.2	286 ±22	270 ±20	0.178
127.5	1.07	15	0.02	1.2	150.3	215 ±19	199 ±17	0.174
127.5	1.09	15	0.02	1.2	150.5	202 ±19	182 ±17	0.170
127.5	1.11	15	0.02	1.2	150.7	163 ±17	143 ±15	0.165
127.5	1.13	15	0.02	1.2	150.9	115 ±15	99 ±12	0.160
127.5	1.15	15	0.02	1.2	151.0	106 ±14	89 ±12	0.156
127.5	1.24	15	0.04	1.65	151.6	110.0 ± 8.4	83.0 ± 6.3	0.138
127.5	1.28	15	0.04	1.65	152.0	94.6 ± 7.8	68.6 ± 5.6	0.131
127.5	1.32	15	0.04	1.65	152.4	89.4 ± 7.7	62.2 ± 5.3	0.124
127.5	1.36	15	0.04	1.65	152.6	85.9 ± 7.6	57.5 ± 5.1	0.117
127.5	1.40	15	0.04	1.65	152.9	88.7 ± 8.0	57.1 ± 5.1	0.110
127.5	1.44	15	0.04	1.65	153.2	90.5 ± 8.3	56.2 ± 5.1	0.104
127.5	1.48	15	0.04	1.65, 1.9	153.5	64.4 ± 4.1	38.6 ± 2.5	0.098
127.5	1.52	15	0.04	1.65, 1.9	153.8	61.2 ± 4.1	35.5 ± 2.4	0.092
127.5	1.56	15	0.04	1.65, 1.9	154.0	50.7 ± 3.9	28.4 ± 2.2	0.086
127.5	1.60	15	0.04	1.9	154.2	40.6 ± 4.7	22.2 ± 2.6	0.081
127.5	1.64	15	0.04	1.9	154.4	44.2 ± 4.5	23.3 ± 2.4	0.076
127.5	1.68	15	0.04	1.9	154.7	30.7 ± 3.8	15.7 ± 1.9	0.071
127.5	1.72	15	0.04	1.9	154.9	37.8 ± 4.4	18.7 ± 2.2	0.066
127.5	1.76	15	0.04	1.9, 2.3	155.1	22.7 ± 2.1	10.9 ± 1.0	0.061
127.5	1.80	15	0.04	1.9, 2.3	155.3	22.3 ± 2.2	10.5 ± 1.0	0.056
127.5	1.84	15	0.04	2.3	155.5	17.6 ± 2.5	8.1 ± 1.1	0.051

TABLE I (*continued*)

$\langle\theta_\pi\rangle_{\text{lab}}$ (deg)	k_{lab} (GeV/c)	$\Delta\theta_{\text{lab}}$ (deg)	$\Delta\theta_{\text{lab}}$ (GeV/c)	E_0 (GeV)	$\langle\theta_\pi\rangle_{\text{c.m.}}$ (deg)	$\langle d\sigma/d\Omega\rangle_{\text{c.m.}}$ (10^{-32} cm^2/sr)	$d\sigma/du$ (10^{-31} [cm/(GeV/c)^2])	u [(GeV/c)^2]
127.5	1.90	15	0.08	2.3	155.9	13.9 ± 1.6	6.1 ± 0.7	0.045
127.5	1.98	15	0.08	2.3	156.3	10.0 ± 1.4	4.2 ± 0.5	0.037
127.5	2.06	15	0.08	2.3, 2.65	156.7	6.68± 0.73	2.7 ± 0.3	0.029
127.5	2.14	15	0.08	2.3, 2.65	157.1	6.56± 0.75	2.5 ± 0.3	0.022
127.5	2.22	15	0.08	2.65	157.4	7.06± 1.05	2.6 ± 0.4	0.017
127.5	2.30	15	0.08	2.65	157.7	8.81± 1.23	3.12± 0.43	0.009
127.5	2.38	15	0.08	2.65, 3.0	158.0	8.19± 0.79	2.77± 0.27	0.004
127.5	2.46	15	0.08	2.65, 3.0	158.2	8.61± 0.87	2.79± 0.28	−0.002
127.5	2.54	15	0.08	3.0	158.5	8.2 ± 1.1	2.58± 0.35	−0.007
127.5	2.62	15	0.08	3.0	158.8	10.6 ± 1.3	3.21± 0.40	−0.012
127.5	2.70	15	0.08	3.0	159.1	9.2 ± 1.2	2.69± 0.36	−0.016
127.5	2.78	15	0.08	3.0	159.4	6.3 ± 1.1	1.79± 0.30	−0.019
127.5	2.86	15	0.08	3.0	159.7	5.7 ± 1.0	1.56± 0.28	−0.022
127.5	2.82	15	0.16	3.5	159.5	4.2 ± 1.4	1.12± 0.34	−0.025
127.5	2.98	15	0.16	3.5	160.1	4.2 ± 1.3	1.10± 0.33	−0.031
127.5	3.14	15	0.16	3.5	160.6	2.0 ± 1.1	0.50± 0.26	−0.037
127.5	3.30	15	0.16	3.5	161.1	1.7 ± 0.9	0.39± 0.20	−0.045
152	1.01	12	0.02	1.3	164.5	203 ±18	202 ±18	0.252
152	1.03	12	0.02	1.3	164.7	187 ±14	181 ±13	0.247
152	1.05	12	0.02	1.3	164.8	153 ±11	145 ±10	0.243
152	1.07	12	0.02	1.3	164.9	135 ±10	124 ±10	0.239
152	1.09	12	0.02	1.3	164.9	126 ±10	112.9 ± 9.0	0.236
152	1.11	12	0.02	1.3	165.0	92.0 ± 8.8	80.7 ± 7.7	0.232
152	1.13	12	0.02	1.3	165.1	94.5 ± 9.1	81.0 ± 7.8	0.229
152	1.15	12	0.02	1.3	165.2	73.5 ± 8.0	61.2 ± 6.7	0.225
152	1.17	12	0.02	1.3	165.3	70.8 ± 8.1	57.9 ± 6.6	0.222
152	1.19	12	0.02	1.3	165.4	70.9 ± 8.0	56.8 ± 6.4	0.219
152	1.21	12	0.02	1.3	165.5	73.3 ± 8.6	57.4 ± 6.7	0.216
152	1.23	12	0.02	1.3	165.6	60.0 ± 7.7	46.0 ± 5.9	0.213
152	1.25	12	0.02	1.3, 1.6	165.7	54.3 ± 5.5	40.5 ± 4.1	0.210
152	1.28	12	0.04	1.6	165.8	48.5 ± 4.6	35.1 ± 3.3	0.206
152	1.32	12	0.04	1.6	165.9	47.1 ± 4.0	32.8 ± 2.8	0.200
152	1.36	12	0.04	1.6	166.1	42.8 ± 3.9	28.5 ± 2.6	0.194
152	1.40	12	0.04	1.6	166.2	41.1 ± 3.9	26.4 ± 2.5	0.188
152	1.44	12	0.04	1.6	166.3	33.2 ± 3.6	20.6 ± 2.2	0.183
152	1.48	12	0.04	1.6, 1.9	166.4	28.1 ± 2.3	16.9 ± 1.4	0.178
152	1.52	12	0.04	1.6, 1.9	166.6	19.6 ± 1.8	11.4 ± 1.1	0.174
152	1.56	12	0.04	1.9	166.7	23.4 ± 2.5	13.2 ± 1.4	0.170
152	1.60	12	0.04	1.9	166.8	16.4 ± 2.3	10.0 ± 1.2	0.166
152	1.64	12	0.04	1.9	167.0	18.2 ± 2.4	9.6 ± 1.2	0.161
152	1.68	12	0.04	1.9	167.1	13.3 ± 2.1	6.8 ± 1.1	0.157
152	1.72	12	0.04	1.9, 2.3	167.2	11.1 ± 1.4	5.52± 0.68	0.154
152	1.76	12	0.04	1.9, 2.3	167.3	9.3 ± 1.2	4.49± 0.60	0.150
152	1.80	12	0.08	1.9, 2.3	167.4	10.0 ± 1.3	4.71± 0.62	0.146
152	1.84	12	0.04	2.3	167.5	10.2 ± 1.7	4.67± 0.78	0.142
152	1.90	12	0.08	2.3	167.7	6.4 ± 1.0	2.73± 0.44	0.138
152	1.98	12	0.08	2.3	167.8	6.0 ± 1.0	2.54± 0.43	0.132
152	2.06	12	0.08	2.3, 2.65	168.0	6.59± 0.73	2.66± 0.29	0.127
152	2.14	12	0.08	2.3, 2.65	168.2	6.70± 0.74	2.59± 0.29	0.121
152	2.22	12	0.08	2.65	168.4	7.46± 1.03	2.75± 0.38	0.116
152	2.30	12	0.08	2.65, 3.0	168.6	6.91± 0.79	2.44± 0.28	0.111
152	2.38	12	0.08	2.65, 3.0	168.8	7.76± 0.80	2.62± 0.27	0.106
152	2.46	12	0.08	2.65, 3.0	168.9	7.12± 0.79	2.31± 0.26	0.101
152	2.54	12	0.08	2.65, 3.0	169.1	6.07± 0.74	1.91± 0.23	0.097
152	2.62	12	0.08	3.0	169.3	6.16± 1.09	1.86± 0.23	0.094
152	2.70	12	0.08	3.0	169.5	4.66± 0.94	1.36± 0.27	0.092
152	2.78	12	0.08	3.0	169.7	3.89± 0.90	1.10± 0.26	0.088
152	2.86	12	0.08	3.0	169.9	2.42± 0.73	0.68± 0.20	0.085

q = average charge collected from quantameter for each event on a roll of film.

The last quantities were constant for a given roll of film but differed from roll to roll.

The position of all the necessary cuts, the SPASS scanning efficiency, and the correction for events beyond the tip of the bremsstrahlung spectrum were all determined from preliminary computer runs. The γ-ray energy bins always extended from just above the inelastic kinematic threshold to approximately $0.97E_0$. The exact positions of the bins were chosen to make the bins from consecutive values of E_0 coincide in the overlap regions and the size of the bins were chosen to be approximately equal to our energy resolution. After it was determined that the cross sections in these overlap regions agreed with each other within statistics, they were averaged using their statistical weighting factors.

The errors in the cross sections are primarily statistical and include the following:

(1) Counting statistics for each bin. In calculating this error, correct account was taken of each event's weighting factor.

(2) The SPASS scanning efficiency, which introduces less than a 2% error in all cases.

(3) The subtraction required to correct for the small residue of events beyond the tip of the bremsstrahlung spectrum that were not eliminated by the data cuts. This introduces an error which varies between $\frac{1}{2}$% for the points taken at the smallest E_0 and production angle and 3% for those at the largest E_0 and production angle.

The remaining errors are primarily systematic. We list here the significant ones, and our estimate of the net uncertainties contributed to the cross sections.

(1) Nuclear absorption correction: ±5%;
(2) Photon flux: ±4%;
(3) Spectrometer solid angle: ±3%.

In addition, there is the possibility that as many as 5%

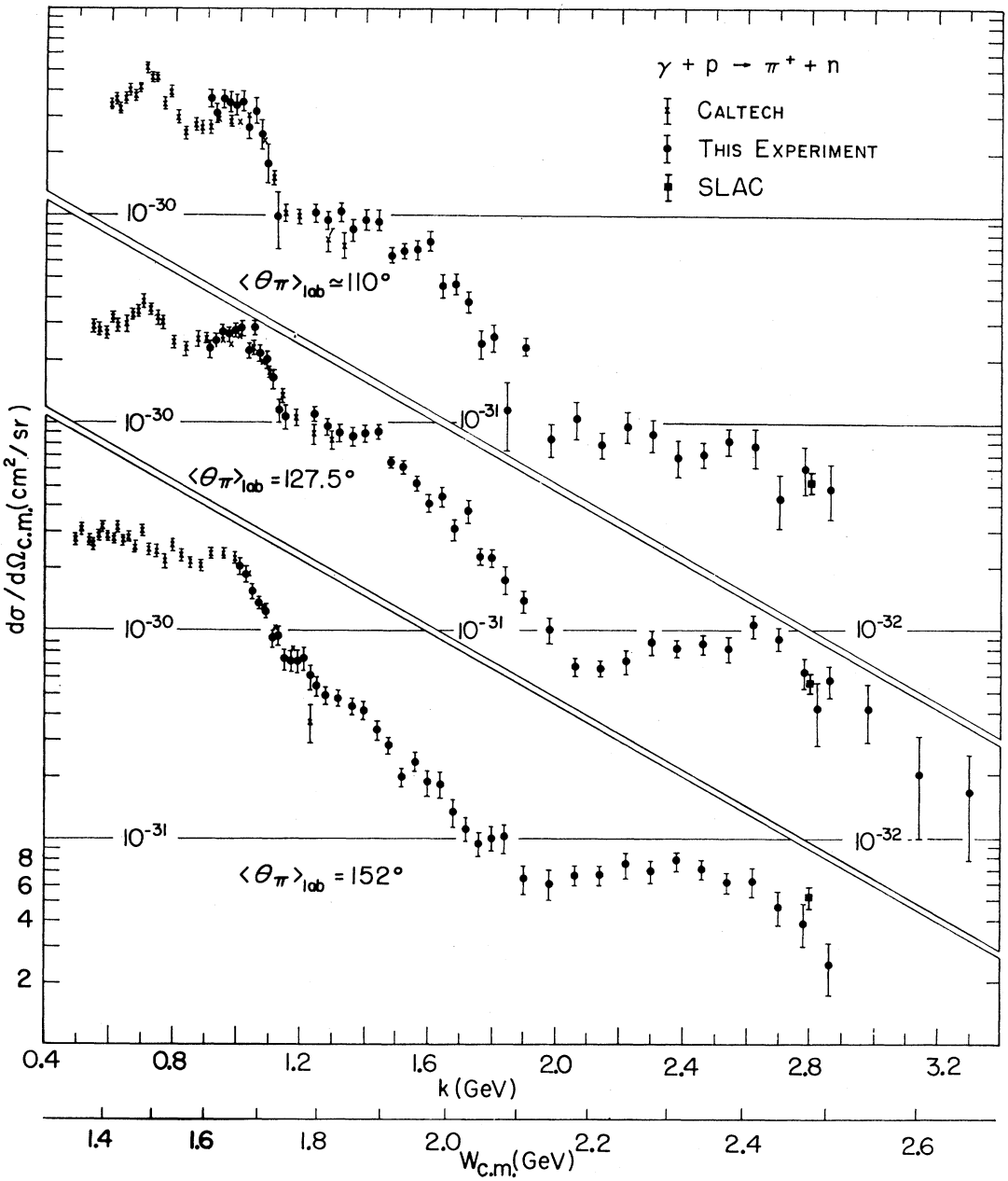

FIG. 9. Differential cross section in the center-of-mass system for the reaction $\gamma+p \rightarrow \pi^+ + n$. Data from other experiments are included (Refs. 5 and 6).

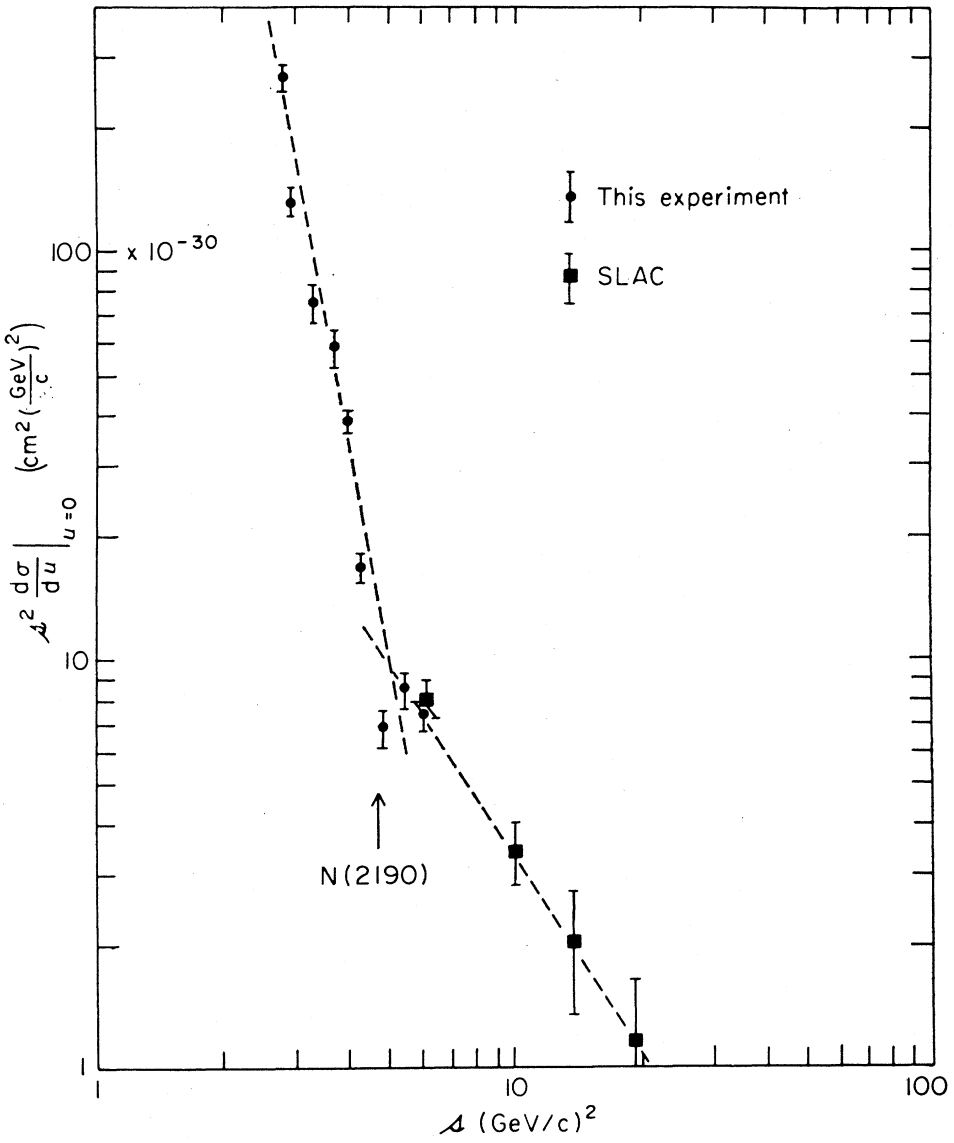

FIG. 10. $s^2 d\sigma/du$ versus s at $u=0$. The data begin to fit Regge models, immediately after the $N(2190)$ resonance. Below this resonance, Regge theory probably cannot be applied.

of the good events might have been eliminated in some bins by the cuts imposed on the data. There is also a possible energy-dependent dead-time effect, due to a fairly high singles rate in counter S_1, of zero to 2%, for which no correction has been made.

IV. RESULTS AND CONCLUSIONS

The results of this experiment are shown in Fig. 9 and are tabulated in Table I. Figure 9 also shows data obtained by others for the same reaction.[6,7] The width of the energy bins for nearly all points extends halfway to the neighboring points; the errors shown in Fig. 9 are statistical only. We have averaged data from several primary beam energies where possible. In all cases, the data from different energies are in good agreement.

There are two main features in our data. First, we see structure in the excitation curves as a function of energy. Second, the general shape of the cross section $d\sigma/du$ shows a rapid decrease with increasing s.

The first feature indicates that the contribution of direct-channel resonances is probably the dominant mechanism for this process in the energy range we have investigated. The well-known resonances $N(1688)$, $\Delta(1920)$, and $\Delta(2420)$ show up as bumps or shoulders in the excitation curves. Their energies appear to be shifted a small amount, due possibly to interference effects which have been noted in other photoproduction

experiments.[2,13,14] The $N(2190)$ resonance does not appear very strongly in these data. The reason for this is not clear and could be owing either to the absence of any photoexcitation of the resonance or to a partial cancellation of the resonant amplitude by the nonresonant background.

Part of the contribution to the nonresonant background could be due to processes such as nucleon or N^* exchange, particularly at large angles in the backward direction. If a simple Regge model is assumed, then the behavior of the cross section for the exchange of a single trajectory might be expected to go as $s^{2\alpha(0)-2}$, where $\alpha(0)$ is the value of $\alpha(u)$ for $u=0$.[15,16] We have plotted $s^2 d\sigma/du$ for $u=0$ as a function of s for our data and those of SLAC[7] in Fig. 10. At energies below the $N(2190)$ resonance our data fall much more rapidly than s^{-2}. For these energies we find that $\alpha(0)=-2.6\pm0.5$, while for the energies above the resonance, our data are consistent with the SLAC data and correspond to $\alpha(0)=-0.45\pm0.08$. This lower value of $\alpha(0)$ is consistent with either nucleon or isobar exchange. The change in slope at the $N(2190)$ resonance would seem to indicate that the resonance amplitude is being excited but appears weakly due to partial cancellation by the nonresonant background amplitude.

[13] C. Schaerf, Nuovo Cimento **44**, 504 (1966).
[14] L. Hand and C. Schaerf, Phys. Rev. Letters **6**, 229 (1961).
[15] R. W. Childers and W. G. Holladay, Phys. Rev. **132**, 1809 (1963).
[16] C. Zweig, Nuovo Cimento **32**, 689 (1964).

ACKNOWLEDGMENTS

We wish to acknowledge the assistance of Dr. G. Voss, the staff of CEA, and the MIT Photoproduction Group of Professor L. S. Osborne. J. Acevedo, A. Nakkasyan, J. Onorato, and J. Schoenwald participated in the data runs and preliminary analysis; E. Ritz wrote much of the momentum analysis program. Professor M. Deutsch provided invaluable assistance in programming and operation of the SPASS measuring system.

PHYSICAL REVIEW D VOLUME 1, NUMBER 7 1 APRIL 1970

Ξ^- Production in 5.5-GeV/c K^-p Interactions*

E. L. GOLDWASSER† AND P. F. SCHULTZ
Department of Physics, University of Illinois, Urbana, Illinois 61801
(Received 19 November 1969)

Final states with a Ξ^- hyperon have been studied in 5.5-GeV/c K^-p interactions. Center-of-mass production angular distributions for the Ξ^- have a peak in the beam direction, while those for the K^+ or K^0 meson peak in the opposite direction. Approximately half of the observed events involve the $\Xi^*(1530)$ or $K^*(890)$ resonances. The four- and five-body final states show production of the $\Xi^*(1930)$ in the $\Xi^-\pi^{+,0}$ mass spectrum and a narrow peak at 2295 MeV in the $\Xi^-\pi^+\pi^-$ mass spectrum. The mass of the Ξ^- hyperon is 1321.9 $\pm$0.5 MeV as determined from 195 Ξ^- decays with a visible Λ decay, assuming a Λ-hyperon mass of 1115.58 MeV.

I. INTRODUCTION

IN this paper we present the results of an investigation of Ξ^- hyperon production in K^-p interactions at 5.5 GeV/c K^- beam momentum. Results of other experiments investigating Ξ^- production have been reported with K^- beam momenta ranging from threshold (1.05 GeV/c) to 10 GeV/c.[1–12]

At our beam momentum, Ξ^-'s are produced in final states containing from two to seven particles and average cross sections are $\sim10\,\mu$b. Consequently, with our beam track length (~4 events/μb), the number of events in any one final state is small, and only the gross features can be observed.

* Work supported by the U. S. Atomic Energy Commission.
† Present address: National Accelerator Laboratory, Batavia, Ill.

[1] J. P. Berge, P. Eberhard, J. R. Hubbard, D. W. Merrill, J. Button-Shafer, F. T. Solmitz, and M. L. Stevenson, Phys. Rev. **147**, 945 (1966).
[2] D. D. Carmony, G. M. Pjerrou, P. E. Schlein, W. E. Slater, D. H. Stork, and H. K. Ticho, Phys. Rev. Letters **12**, 482 (1964).
[3] P. M. Dauber, J. P. Berge, J. R. Hubbard, D. W. Merrill, and R. A. Muller, Phys. Rev. **179**, 1262 (1969).
[4] G. Burgun, J. Meyer, E. Pauli, B. Tallini, J. Vrana, A. de Bellefon, A. Berthon, K. L. Rangan, J. Beaney, M. U. Deen, C. M. Fisher, and J. R. Smith, Nucl. Phys. **B8**, 447 (1968).
[5] G. W. London, R. R. Rau, N. P. Samios, S. S. Yamamoto, M. Goldberg, S. Lichtman, M. Primer, and J. Leitner, Phys. Rev. **143**, 1034 (1966).
[6] J. Badier, M. Demoulin, J. Goldberg, B. P. Gregory, C. Pelletier, A. Rouge, M. Ville, R. Barloutaud, A. Leveque, C. Louedec, J. Meyer, P. Schlein, A. Verglas, D. J. Holthuizen, W. Hoogland, and A. G. Tenner, Phys. Letters **16**, 171 (1965).
[7] Birmingham-Glasgow-London (I.C.)-Oxford-Rutherford Collaboration, Phys. Rev. **152**, 1148 (1966).
[8] G. S. Abrams, R. G. Glasser, B. Kehoe, B. Sechi-Zorn, and G. Wolsky, Phys. Rev. **175**, 1697 (1968).
[9] J. Alitti, E. Flaminio, W. Metzger, D. Radojičić, R. R. Rau, N. P. Samios, I. Skillicorn, C. R. Richardson, D. Bassano, M. Goldberg, and J. Leitner, Phys. Rev. Letters **21**, 1119 (1968).
[10] J. Alitti, V. E. Barnes, E. Flaminio, W. Metzger, D. Radojičić, R. R. Rau, C. R. Richardson, N. P. Samios, D. Bassano, M. Goldberg, and J. Leitner, Phys. Rev. Letters **22**, 79 (1969).
[11] Aachen-Berlin-CERN-London (I.C.)-Vienna Collaboration, Nucl. Phys. **B4**, 326 (1968).
[12] Aachen-Berlin-CERN-London (I.C.)-Vienna Collaboration, Phys. Letters **28B**, 439 (1968).